EXPERIMENTAL STUDY OF GAS ENTRAINMENT FROM SURFACE SWIRL

B. Moudjed, J. Excoffon, R. Riva and L. Rossi
CEA Saclay, DEN/DANS/DM2S/STMF/LIEFT, Laboratoire d'Instrumentation et d'Expérimentation en mécanique des Fluides et Thermohydraulique, F-91191 Gif-sur-Yvette Cedex, France.
brahim.moudjed@cea.fr (brahim.moudjed@yahoo.fr), jacques.excoffon@cea.fr, roland.riva@cea.fr, lionel.rossi@cea.fr

ABSTRACT

This work addresses the general topic of the gas entrainment from a free surface by a swirl issued from the pumping of fluids below the free surface. This phenomenon is investigated through an analytical experiment in water called BANGA. A shear flow is generated between a horizontal flow and a stagnant flow. At the bottom of the test section, a vertical pumping is added to produce gas entrainment. One particularity of these experiments is the possibility to change the shape of the channel generating the inlet conditions by adding obstacles so as to trigger different conditions for the turbulent shear flow. Three geometries of obstacles are used: a square block, a half cylinder and a ramp. Depending on the flow conditions, a surface swirl can be created with a sufficient strength to entrain gas below the free surface to the vertical pumping outlet. Gas entrainment onset for the plane plate is the highest in terms of suction velocity for the lowest inlet velocities. The frequency of gas entrainment occurrence is measured using visualizations of the flow. Two entrained regimes are identified for low and high Reynolds number flows: the surface swirl induced gas entrainment in its core reaching the suction nozzle and bubbles issued from the breaking of the gas core are pumped.

KEYWORDS
Gas entrainment, Surface swirl, Flow visualization

1. INTRODUCTION

Gas entrainment has been identified as one of the main sources of safety issue in the Sodium cooled fast reactor (NaSFR). It can generate transport of a large quantity of gas through the core and lead to the accumulation of gas pockets close to the core of the reactor [1, 2]. Such behavior is induced by both the presence of eddies at the free surface and the downward flow created by the suction of hot liquid sodium by the intermediate heat exchanger.
To investigate such behavior, many experimental facilities were performed mainly in water.
Baum *et al*. [3] begins to study the problem through a cylindrical glass apparatus where the eddy structure is generated by introducing the flow with a tangential inlet pipe. The liquid exits through an outlet pipe at the center of the bottom of the cavity. Four liquids were investigated (water, white spirit, Freon 113 and sodium) to detect the onset of gas entrainment and demonstrate that surface tension play a major role in gas entrainment.
Flow mechanisms of air entrainment was also studied by Takahashi *et al*. [4] through an experimental set up close to that used by Baum *et al*. and with the possibility to add a forced circulation by turning the cylindrical cavity. In particular, they found that an air core with break up bubbles changes to a continuous air core with an additional forced circulation.
A few years later, the scale effect was studied by Eguchi *et al*. [5] with different kind of water so that Reynolds and Froude numbers change by modifying the viscosity, the inlet velocity, the inlet size and the

water level. They showed that gas entrainment inception appears earlier when the Reynolds number increases and that increasing the Froude number tends to delay gas entrainment onset.
In all these experimental investigations, the gas entrainment is maintained continuously whereas it appears intermittently in NaSFR. To study intermittent gas entrainment, new experiment facilities, mainly in water, has then been designed in more recent studies as Ezure *et al*. [6, 7], Kimura *et al*. [8][*] or Cristofano *et al*. [9].
These experiments are based on an open channel flows where the main flow is separated from a water dead zone with vertical plates at the inlet and outlet parts. This setup generates a shear flow in the central area. A suction nozzle set at the center bottom of the channel allows to generate a downward flow in order to induce intermittent gas entrainment. They provide both the occurrence map of gas entrainment with respect to experimental conditions through the inlet velocity, the outlet velocity and the suction velocity. Kimura *et al*. [8] have also investigated the case of the sodium whose geometry of the test section is the same as than in water to demonstrate that water experiments simulated well the onset conditions of gas entrainment in sodium. Agreements found between experiments support the suitable use of water to understand the physics of surface eddies and gas entrainment occurring in sodium.
In addition, Kimura *et al*. [10] have performed experiments in a partial model of the Japan Sodium cooled Fast Reactor (build to 1/1.8scale) which shows that gas entrainment result from the wake of obstacles and the presence of shear flow.

The present study focuses on gas entrainment occurrence in water. The geometry of the experimental channel is close to that of Ezure *et al*. [6, 7] and Kimura *et al*. [8]. The main difference lies in the inlet conditions. In particular, obstacles can be added so that present experiments link the approaches pursued with a rectangular water tank [6 - 8] and with a partial reduced model of Sodium cooled fast reactor [10].
The main objectives are firstly, to identify the inlet and suction condition of gas entrainment occurrence and secondly, to characterize the gas entrainment occurrence frequencies. Among the experimental parameters, the geometry of the inlet channel is varied by changing the obstacle shape.

2. EXPERIMENTAL SET UP

2.1. Experimental rig

Free surface flows are performed within a 700mm length and 108mm width rectangular channel filled with water (210mm height): see figure 1. It is integrated in a close loop which includes a pump, a thermal exchanger, temperature probes, flowmeters and valves.
As depicted in figure 1, two vertical plates are placed in the middle of the channel so that inlet and outlet flows are limited to a part of the channel cross-section. These plates are separated from 300mm. A 50mm diameter suction nozzle, with a height of 100m[*], is set at the bottom of the cavity to induce a secondary down-flow by pumping the water under the free surface.
The investigated area is the central part of the test section with dimensions 300 x 108 x 110 mm^3.

The geometry of the present channel is different from the channel used by Ezure *et al*. [6, 7] or Kimura *et al*. [8]. For these two last authors, the flow is vertically injected from the bottom in a water tank before being conducted to the channel (see fig. 3a). For the present study, the inlet flow is horizontally generated through circular pipe linked to a segmented divergent followed by an intermediate chamber. A grid with 1mm diameter circular holes, is set between the divergent and the chamber (see fig. 3b) so as to prevent flow separation.

[*] Ezure *et al*. and Kimura *et al*. use the same experimental facility with a test apparatus of different size namely, a rectangular cavity of 300mm width for the first and of 100mm width for the second.
[*] 110mm from the free surface.

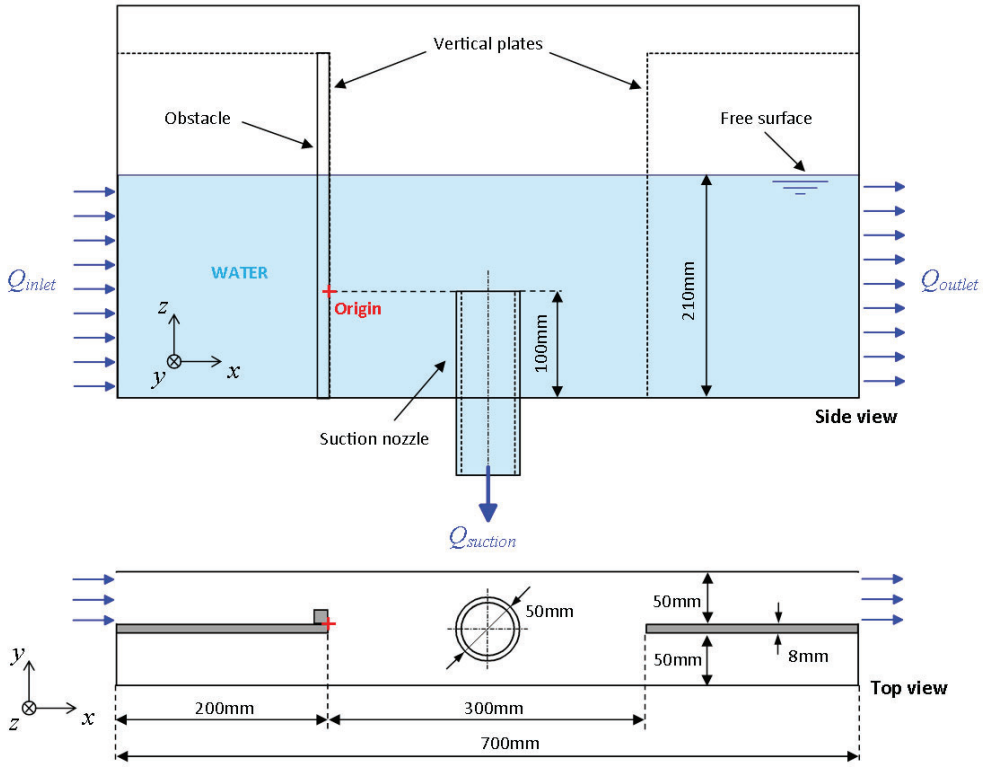

Figure 1. Experimental set up: side view at the top and top view at the middle. Origin of the Cartesian frame is set on the border of the vertical plate at the height of the suction nozzle: *x*-axis coincides with the horizontal main flow, *y* and *z* axis are respectively horizontal and vertical.

Velocity profiles were measured with the LDA (Laser Doppler Anenometry) technique to verify that the inlet flow is parallel. Figure 3 provides the dimensionless horizontal velocity profile V_x / $V_{x\ mean}$ measured at the inlet of the test section; $V_{x\ mean}$ = 16cm/s is the mean velocity. The standard deviation of V_x / $V_{x\ mean}$ is about 7%.

Eventually, experiments are performed without and with obstacles of different shapes and sizes. Three geometries of obstacle are used to modify the shape of the inlet channel: a square block as an academic case, a half cylinder to get closer to the control bar shape and a ramp to increase gradually the inlet flow rate; they are represented in figure 2. The obstacle heights are set to 12,5mm and 25mm; in the present paper, only the case of 12,5mm will be investigated.

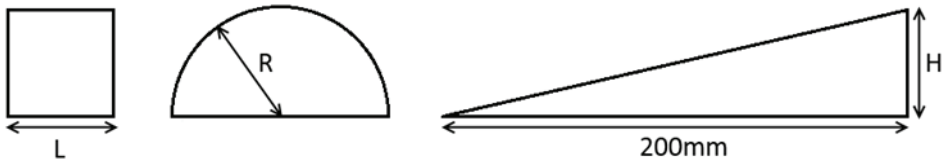

Figure 2: Sketch of the obstacles

2.2. Experimental methods

The experimental investigations are conduct through two stages:

- flow visualizations (observations, high speed camera, frame acquisition),
- velocity measurement (LDA, PIV).

Visualizations in white light are firstly performed to evaluate the gas entrainment occurrence. A *Stemmer Imaging*™ camera, with a spatial resolution of 2048 x 1088 pixels, is used to acquire frames with a frequency of 25Hz during 15min. Viewed area is 36cm long and 19cm wide and includes both the free surface and the suction nozzle. A treatment is then applied to the images to evaluate the gas entrainment occurrence frequencies. This treatment is based on the contour detection to recognize entrained air volumes and uses the well know Canny method [11] which detect edges evaluating gray scale gradient.

Spatial and temporal structure of the flow is then characterized in term of velocity field with the PIV (Particle Image Velocimetry) technique. The purpose is to firstly, characterize the structure and the nature of the flows, secondly, compare the flow conditions leading to gas entrainment according to different parameters and thirdly, identify the physical phenomenon responsible for the gas entrainment so as to quantify the different mechanisms involved, their role and dominance according to different flow regimes.

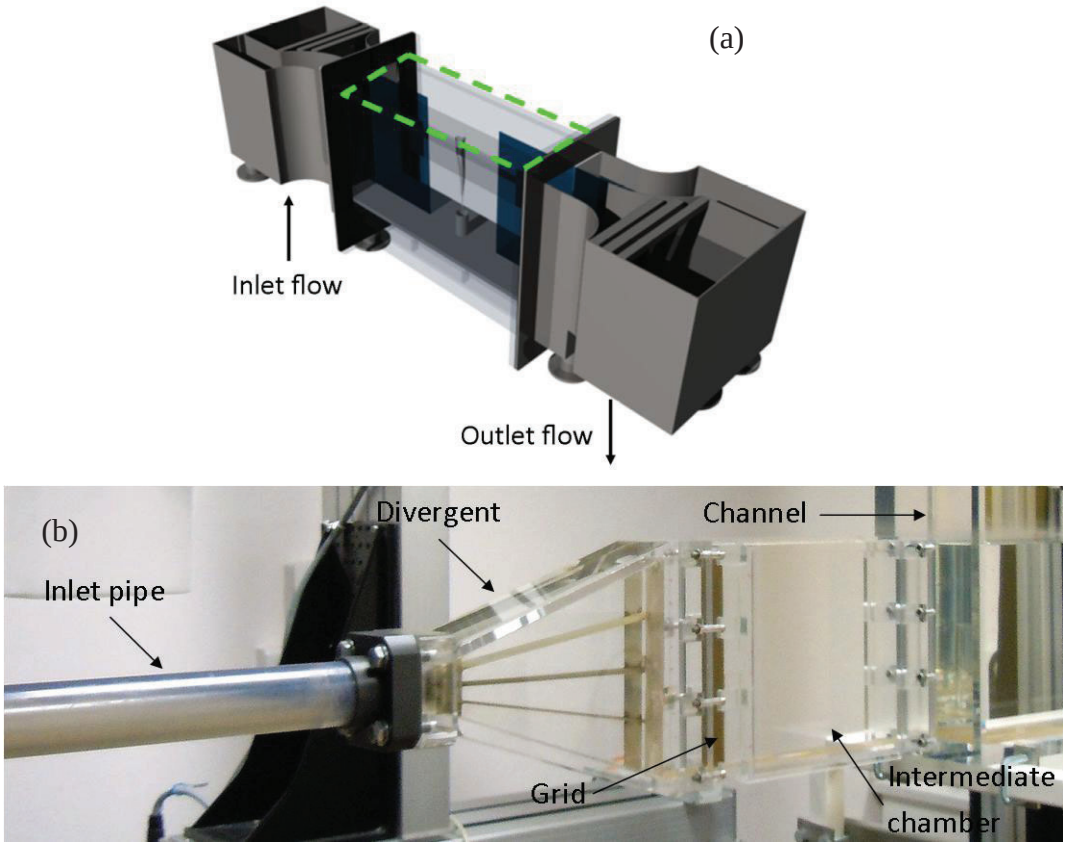

Figure 3: (a) experimental set-up of Ezure *et al*. [6, 7] and Kimura *et al*. [8], and (b) photo of the inlet equipment for the channel of the present study.

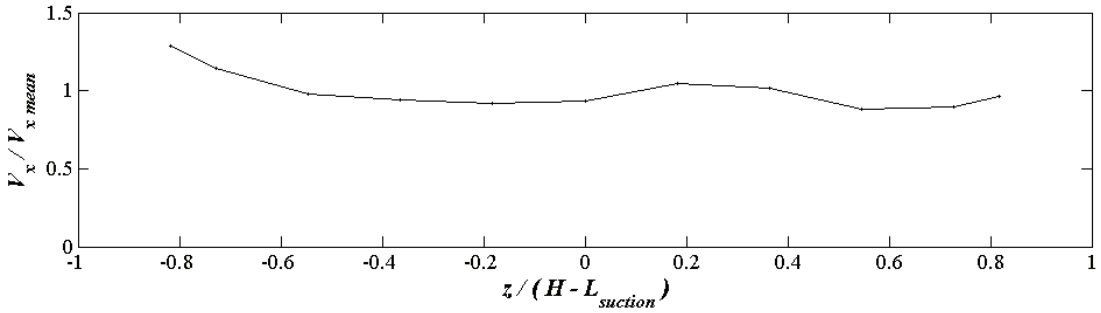

Figure 4. Dimensionless horizontal velocity $V_x / V_{x\,mean}$ is plotted at x = - 180mm and y = 30mm, as function of dimensionless vertical distance $z / (H - L_{suction})$, with H, the water depth and $L_{suction}$, the length of the suction nozzle, so that $(H - L_{suction}) = 110$mm.

3. RESULTS AND DISCUSSIONS

Five inlet flow rates are selected between 1.9 and 9.5m^3/h. The inlet flow rate Q_{inlet} is measured with a flowmeter so that the inlet velocity V_{inlet} is defined as $V_{inlet} = Q_{inlet} / (L \,.\, H)$, where L represents the width of the inlet channel and H, the water depth. Likewise, the suction flow rate $Q_{suction}$ is measured with a flowmeter so that the suction velocity $V_{suction}$ can be estimated as $V_{suction} = Q_{suction} / (\pi r^2)$ with r, the suction nozzle radius.

Observations of five minutes are firstly performed to determinate if gas entrainment occurs or not. The geometries of the obstacles and the flow rates Q_{inlet} and $Q_{suction}$ are varied. Figure 5 provides the gas entrainment map for the three obstacles and threshold lines are reported in figure 6. Inception of gas entrainment varies with respect of obstacle in terms of suction velocity: the ramp seems to advance gas entrainment occurrence whereas the square block seems to delay it. The case of the plane plate is also plotted both for the present study and for Kimura *et al*. [8]: threshold are very close and crossed cases with obstacles. From these observations, key parameters, namely inlet and suction flow rate, are selected to evaluate the gas entrainment occurrence frequency: they are listed in table I.

Visualizations of the flow are then performed during fifteen minutes in white light. Figure 7 provides snapshot of two different sets of inlet and suction flow rates for the square block. Two ways of gas entrainment can be identify: bubbles separation from a non-continuous surface swirl (fig. 7a, 7c) and continuous surface swirl reaching the suction nozzle (fig. 7b, 7d). Moreover, it can be noted that the shape of the surface swirl and the entrained air bubbles vary with the flow regime determined by the Reynolds. The Reynolds number Re is defined as: $Re = (V_{inlet} \,.\, L) / \nu$, with V_{inlet}, the inlet velocity, L, the characteristic length of the obstacle (the side length for the square block, the radius for the half cylinder and the height for the ramp) and ν, the kinematic viscosity of the water ($\nu = 10^{-6}$m^2/s). Surface swirls are wider for high (fig. 7c, 7d) than for low (fig. 7a, 7b) Re number: Re = 6250 and 3750, respectively. Gas entrainment seems also stronger and more disordered, in terms of bubbles structures for the case of high Reynolds number (fig. 7c, 7d).
The Froude number Fr expressed as: $Fr = V_{inlet} / (gH)^{½}$, with g, the gravitational acceleration (g = 9.81m/s^2) and H, the water depth, is between 0.1 to 0.2 for the snapshot in figure 7.
Another dimensionless key parameter is the Weber number We defined by: $We = (\rho V_{inlet}^2) / (\sigma / l_{swirl})$,
where ρ represents the density (ρ = 1000kg/m^3 for water) , σ, the surface tension ($\sigma \approx$ 70N/m^3 for the water) and l_{swirl}, the surface swirl diameter just under the free surface. Weber number for cases of figure 7b and figure 7d is respectively about 7 and 31, that is to say with a factor 4.

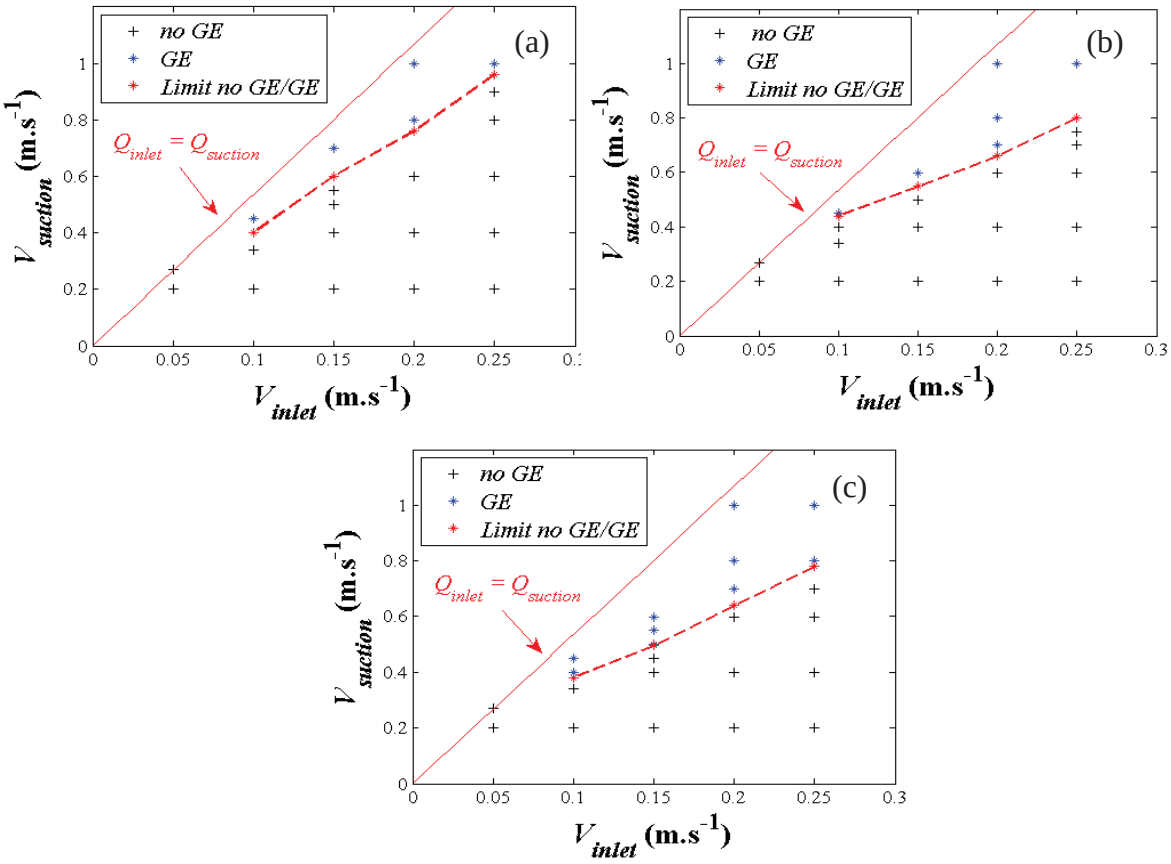

Figure 5. Occurrence maps of gas entrainment onset for (a) the square block, (b) the half cylinder and (c) the ramp. The red dashed lines represent the gas entrainment threshold. The solid red lines correspond to $Q_{inlet} = Q_{suction}$. Cases with and without gas entrainment are respectively plotted with black crosses and blue stars.

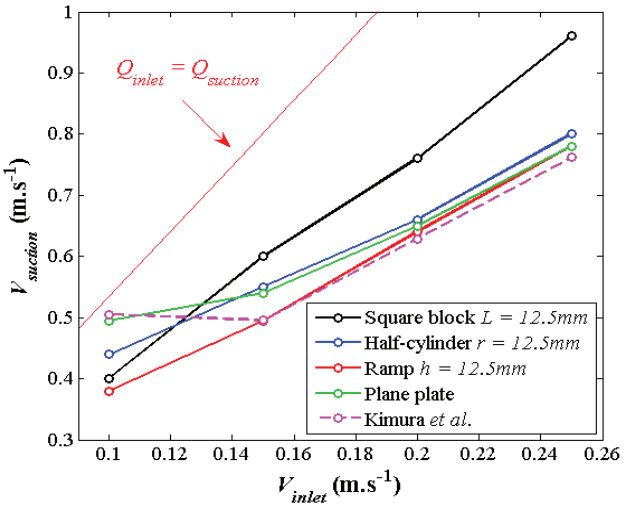

Figure 6. Onsets of gas entrainment for the three geometries and the plane plate of the present study, and for experimental points of Kimura *et al.* [8].

Table I. Inlet and suction parameters.

Q_{inlet} ($m^3.h^{-1}$)	V_{inlet} ($m.s^{-1}$)	$Q_{suction}$ ($m^3.h^{-1}$)	$V_{suction}$ ($m.s^{-1}$)
1.9	0.05	1.9	0.27
3.8	0.1	2.8	0.4
		3.2	0.45
5.7	0.15	3.6	0.5
		4.2	0.6
		4.9	0.7
7.6	0.2	4.2	0.6
		5.7	0.8
		7.1	1
9.5	0.25	4.2	0.6
		5.7	0.8
		7.1	1

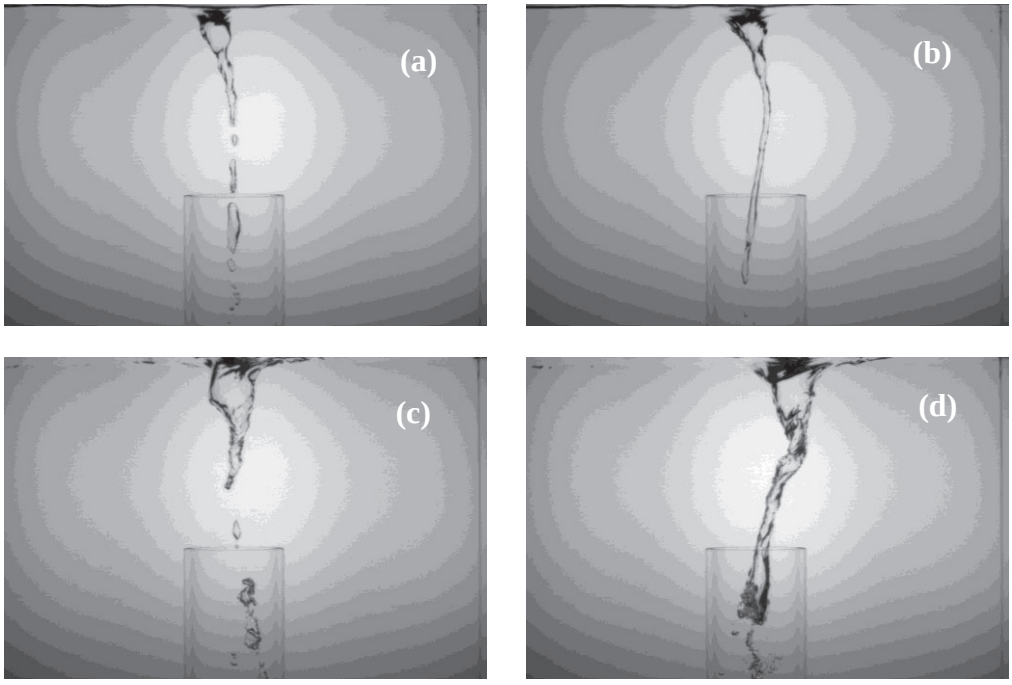

Figure 7. Snapshot of Non continuous Surface swirls and gas entrainments for (a) Q_{in} = 5.7m^3/h, $Q_{suction}$ = 4.9m^3/h and (c) Q_{in} = 9.5m^3/h, $Q_{suction}$ = 7.1m^3/h. Snapshot gas entrainment trough Continuous Surface swirls for (b) Q_{in} = 5.7m^3/h, $Q_{suction}$ = 4.9m^3/h and (d) Q_{in} = 9.5m^3/h, $Q_{suction}$ = 7.1m^3/h.

4. CONCLUSIONS

This work presents an experimental investigation of the gas entrainment in a channel flow with a free surface. Gas entrainment onset are comparable, in terms of suction velocity, for the plane plate, the half cylinder and the ramp for high inlet velocity. Moreover, it can be noted that gas entrainment inception with the plane plate is similar for the present study and experiments of Kimura *et al*. [8]. Two way of gas entrainment have been identified: through continuous and non-continuous surface swirl. Structure of surface swirl and air bubbles depends on the flow regime determined by the Reynolds number. They respectively seem wider and more disordered for high than for low *Re*.
Results of count have not been presented here and should be presented in our talk.
Further investigations are focusing on the characterization of the complete velocity field according to geometries and sizes of obstacles and flow regimes, through PIV measurements. We aim, in particular, to identify the turbulent structures and to quantify the more relevant physical parameters in order to explain the physical mechanisms responsible for this intermittent phenomenon of gas entrainment.

ACKNOWLEDGMENTS

The authors would like to acknowledge Muriel Marchand, a CEA colleague, for her involvement in the development of BANGA.

REFERENCES

[1] D. Tenchine, “Some thermal hydraulic challenges in sodium cooled fast reactors,” *Nucl. Eng. Des.*, **240(**5), pp. 1195–1217 (2010).
[2] D. Tenchine, C. Fournier, and Y. Dolias, “Gas entrainment issues in sodium cooled fast reactors,” *Nucl. Eng. Des.*, **270**, pp. 302–311 (2014).
[3] M. R. Baum and M. E. Cook, “Gas entrainment at the free surface of a liquid: entrainment inception at a vortex with an unstable gas core,” *Nucl. Eng. Des.*, **32**(2), pp. 239–245 (1975).
[4] M. Takahashi, A. Inoue, M. Aritomi, Y. Takenaka, and K. Suzuki, “Gas Entrainment at Free Surface of Liquid, (I),” *J. Nucl. Sci. Technol.*, **25**(2), pp. 131–142 (1988).
[5] Y. Eguchi and N. Tanaka, “Experimental study on scale effect on gas entrainment at free surface,” *Nucl. Eng. Des.*, **146**(1–3), pp. 363–371, (1994).
[6] T. Ezure, N. Kimura, K. Hayashi, and H. Kamide, “Transient Behavior of Gas Entrainment Caused by Surface Vortex,” *Heat Transf. Eng.*, **29**(8), pp. 659–666 (2008).
[7] T. Ezure, N. Kimura, H. Miyakoshi, and H. Kamide, “Experimental investigation on bubble characteristics entrained by surface vortex,” *Nucl. Eng. Des.*, **241**(11), pp. 4575–4584 (2011).
[8] N. Kimura, T. Ezure, H. Miyakoshi, H. Kamide, and T. Fukuda, “Experimental Study on Gas Entrainment Due to Nonstationary Vortex in a Sodium Cooled Fast Reactor - Comparison of Onset Conditions Between Sodium and Water,” presented at the *17th International Conference on NuclearEngineering*, Brussels Belgium (2009).
[9] L. Cristofano, M. Nobili, and G. Caruso, “Experimental study on unstable free surface vortices and gas entrainment onset conditions,” *Exp. Therm. Fluid Sci.*, **52**, pp. 221–229 (2014).
[10] N. Kimura, T. Ezure, A. Tobita, and H. Kamide, “Experimental Study on Gas Entrainment at Free Surface in Reactor Vessel of a Compact Sodium-Cooled Fast Reactor,” *J. Nucl. Sci. Technol.*, **45**(10), pp. 1053–1062 (2008).
[11] J. Canny, “A Computational Approach to Edge Detection,” *IEEE Trans. Pattern Anal. Mach. Intell.*, **PAMI-8**(6), pp. 679–698 (1986).